Received: Added at production | Revised: Added at production | Accepted: Added at production

DOI: xxx/xxxx

RESEARCH ARTICLE

Wind turbine main-bearing loading and wind field characteristics

Edward Hart*[1] | Alan Turnbull[1] | Julian Feuchtwang[1] | David McMillan[1] | Evgenia Golysheva[2] | Robin Elliott[2]

[1]Wind and Marine Energy Systems CDT, University of Strathclyde, Glasgow, UK
[2]Onyx InSight, University of Nottingham Innovation Park, Nottingham, UK

Correspondence
*Edward Hart, Wind and Marine Energy Systems CDT, University of Strathclyde, Glasgow, UK. Email: edward.hart@strath.ac.uk

This work was funded by the EPSRC under project reference number EP/L016680/1.

Abstract

This paper investigates the relationship between wind turbine main-bearing loads and the characteristics of the incident wind field in which the wind turbine is operating. For a 2MW wind turbine model, fully aero-elastic multibody simulations are performed in 3D turbulent wind fields across the wind turbine's operational envelope. Hub loads are extracted and then injected into simplified drivetrain models of three types of main-bearing configuration. The main bearing reaction loads and load ratios from the simplified model are presented and analysed. Results indicate that there is a strong link between wind field characteristics and the loading experienced by the main-bearing(s), with the different bearing configurations displaying very different loading behaviours. Main-bearing failure rates determined from operational data for two drivetrain configurations are also presented.

KEYWORDS:
Wind turbine, bearings, main-bearing, load modeling, aero-elastic simulation

1 | INTRODUCTION

The rate of wind turbine main-bearing failures is high, with most not reaching their design lives of roughly 20 years, and in some cases failing in less than six years [1]. The reasons for this are multi-faceted and as yet not fully understood; a contributing factor undoubtedly being the fact that conditions experienced by main-bearings inside a wind turbine drivetrain deviate significantly from the well understood and relatively constant conditions present in conventional energy plant generators. It is in these latter and altogether more hospitable conditions where much of the current main-bearing knowledge base has been developed and, when dealing with wind turbines, there is generally an implicit assumption that this prior experience can be reapplied without much alteration. The relatively high proportions of main bearing failures seen in the field suggest that these assumptions need to be revisited. This paper seeks to both challenge these assumptions and attempt to shed some light on the problem by addressing the following question:

What range of load conditions are experienced by a wind turbine main-bearing across its operating envelope and to what extent can these load conditions be linked to characteristics of the incident wind field?

Inroads to answering this question have been made [2,3] and the current paper pulls this previous work together, while extending the analysis performed to date and including a third drivetrain configuration. Failure rates, based on operational data from over 2000 turbines, for turbines with two of the analysed main-bearing configurations are also given.

[0]**Abbreviations:** SMB, single main-bearing; DMB, double main-bearing; CPLS, common parameter load set; SE, shear exponent; TI, turbulence intensity.

2 | BACKGROUND

Relatively few studies exist in the literature which consider realistic main-bearing loading, load modeling, or which look at the underlying load conditions which lead to the various damage modes seen in the field. Most wind turbine main-bearing research focuses on the detection of a fault after it has occurred [4], however, in this example the analysis does not consider realistic load conditions, but rather contact stresses with and without a fault present. The analysis [4] is also based on theory developed for generic low-speed shaft bearings [5], rather than being specific to wind turbines. Another study [6] considers main-bearing fault detection by looking to detect increased axial vibration amplitudes on the LSS which are assumed to result from reduced bearing axial stiffness caused by damage to the bearing. A recent field study [7], also concerned with fault detection, applied artificial neural networks to SCADA data in order to detect main bearing faults. A 'normal behaviour model' is first constructed using healthy turbine data, with future deviations from the predicted behaviour indicating a possible fault. The variables used to build the model are: bearing temperature, ambient temperature, power and rotational speed. Results of this work seem promising with warnings generated between 10 and 3.5 months before observed failures and alarms activated between 2.5 months and 3 days before failures. Main-bearing reliability has also been considered from a data-driven perspective [9] in order to inform inspection and maintenance decisions.

A dynamic lubrication control system has been proposed [8] which could theoretically supply the correct quantity of lubricant, in real-time, to the main-bearing in order to keep the lubricating film thickness at its optimal value for the current main-bearing loading. However, in the formulation of this method, the main-bearing loads are linked to the power output of the wind turbine according to the design loading at a given wind speed. This method therefore implicitly assumes a uniform wind speed across the rotor and ignores the effects of both shear and turbulence. The results of the current paper demonstrate that the main-bearing loads are sensitive to both turbulence and wind shear and so indicate that while the essential philosophy is sound, a more detailed consideration of main bearing operational loads will be required for their method to be practical in the field.

An NREL study [1] considers realistic main-bearing loading using SIMPACK multibody simulation software in order to optimise main-bearing design. This uses 11 hub load time-histories to represent loading across the wind turbine's operational envelope, the current paper will consider more loading conditions with 24 types of wind field and 6 generated of each type, resulting in a total of 144 loading time histories. In the current paper, these large numbers of loading conditions are possible due to the simplified drivetrain models developed here, with the low number of load cases in the NREL study likely due to higher computational times for the more complex SIMPACK model. For the case of a direct-drive floating wind turbine, a multibody model of the main-bearing has been defined [10] which can analyse tapered roller loads and the effects of shaft misalignment. The model is general enough that it should be possible to alter it for geared and/or non-floating turbine cases in the future. The work itself doesn't consider dynamic operational loading but instead applies the rotor weight to the shaft and increases axial forces linearly as a proxy for wind loading across the rotor. The results are shown to agree well with a reference model and hence the presented models show good potential for an analysis tool under dynamic input loads. However, the complexity of model will limit the number of load time-history analyses which could be performed in reasonable time.

Apart from the works mentioned here there is really very little else in the wind turbine main-bearing literature, with most other information existing in industry white papers [11]. This is worrying considering the fact that main-bearing replacement costs can be as high as that of gearboxes [9] (an area which receives a great deal more attention, as will be outlined below); as wind turbine assets grow in size these costs are also likely to rise due to the need for the entire rotor to be supported during main-bearing replacement. Apart from the costs of the repairs themselves, main-bearing failures will also result in lost revenue, from a non-producing turbine, until repairs are completed. As mentioned above, it is notable that most research efforts to date which consider the main-bearing are focused on fault diagnosis and prognosis, with the areas of failure root-cause, realistic load modelling and design and operational implications conspicuously absent. Wind turbine gearboxes on the other hand have received considerable attention in terms of loads, load modeling and the relationship to damage modes. For example there are papers dealing specifically with gearbox bearing loads in relation to bearing slippage, load measurements, wind shear effects on planetary bearing loads and contact load fatigue for planetary bearings [12,13,14,15]. The papers mentioned here are just some examples from what is easily described as a vast literature on the subject. It would therefore seem that there is a considerable knowledge gap when it comes to wind turbine main-bearing science. In response to this, the current paper is looking to both motivate and initiate the filling of this knowledge gap.

3 | FAILURE DATA ANALYSIS

Along with the relatively small number of studies performed to date which focus on wind turbine main-bearings, there is a corresponding lack of data detailing main-bearing failure rates, both at a high level and also with respect to specific bearing configurations. In order to motivate the current study, and also to allow for main-bearing issues to be highlighted more generally, Onyx InSight have made failure rates available to this work for both single and double main-bearing drivetrain configurations. In order to provide a reasonable comparison, two turbines were selected which are both rated in the range of 1.5-2.5 MW. One has a single main-bearing (SMB) drivetrain while the other has a double main-bearing (DMB). The operational

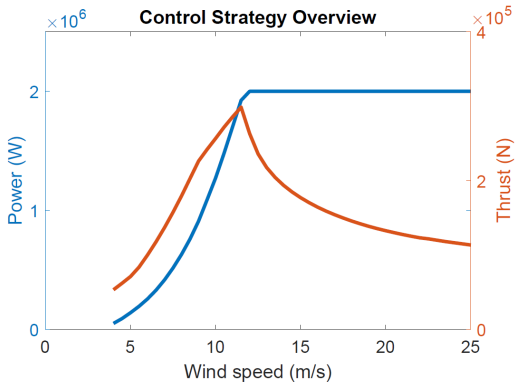

FIGURE 1 Turbine designed power and thrust curve against wind speed.

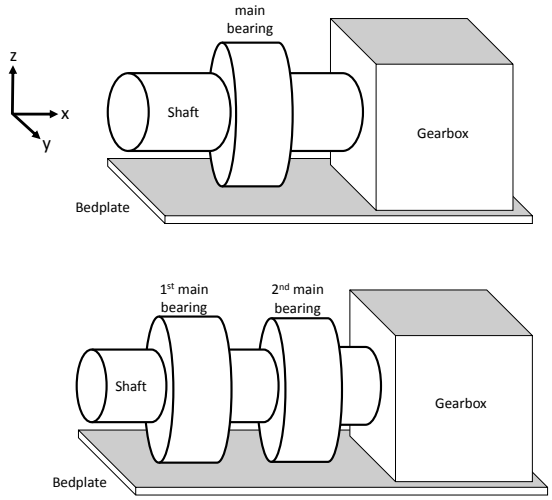

FIGURE 2 Main-bearing schematic for single and double bearing configurations. The reference frame is also given.

data used for this analysis includes over 1000 turbines of each type. Based on this data main-bearing failure rates, presented as 20 year (i.e. lifetime) failure rates, were found to be roughly 30% for the SMB turbines and 15% for the DMB turbines. And hence, in this case, the SMB turbines have been found to fail with around twice the frequency of the DMB turbines. One must avoid extrapolating too far with this data however, due to the fact that there will be contextual factors (such as control and operating environments) other than the main-bearing configuration which might be driving these failure rates. With respect to the current work the conclusions drawn from these figures are:

1. Main-bearing failure rates are higher than might be expected
2. Different main-bearing configurations might lead to significantly different failure rates.

With respect to fatigue loading, wind turbine main bearings should be lasting well over 20 years [16]. This, combined with the observation that main-bearing operating conditions in wind turbines are very different from those under which the rolling element knowledge base has historically developed, implies that it may well be other forms of damage, and not fatigue mechanisms, which are the main drivers of main-bearing life. These other damage mechanisms generally take the form of wear and tear, due to operating outside of design limits, with the most prevalent forms of roller bearing damage coming from:

1. Bearing misalignment due to overly high loading, resulting in physical damage (grooves, pits and cracks) and wear particles being introduced to the lubricant [17,18]
2. High axial to radial load ratios leading to bearing unseating, skewing and sliding [1,11]; this leads to damage modes related to abrasion and wear micro-pitting from raceway-roller interactions [19].

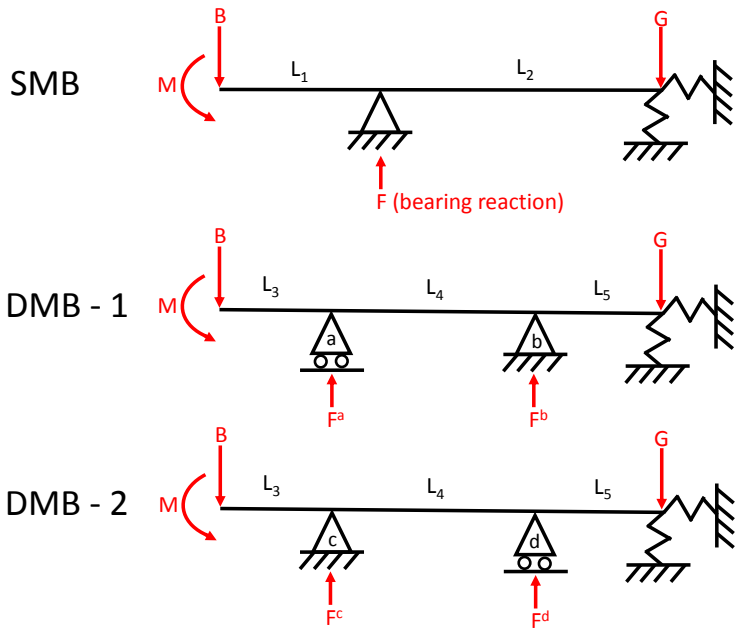

FIGURE 3 Main-bearing models for each pair of in-plane force-moment pairs. Note that G is the gearbox weight in the vertical plane and zero in the horizontal plane.

This work therefore focuses on bearing loading characteristics which can contribute to the wear mechanisms outlined above. The load types considered are therefore **mean loading**, **peak loading** and axial-to-radial **load ratios**. Note that while classical fatigue approaches to rolling element lifetime are dependent on numbers of cycles, and hence evaluated in the frequency domain, the mechanism under investigation in the current work can initiate damage in a single or small number of load events. Therefore, rather than a frequency domain analysis we instead consider the expected values of selected load types across multiple simulations at given operating points and wind conditions, with a higher expected value of load type assumed to indicate a higher risk of damage for the given conditions.

Given the large disparity in lifetime failure rates for SMB and DMB drivetrains reported above, this work also looks to compare loading results for these two drivetrain types in order to determine if any insight can be gleaned with respect to the reported figures. While the current work considers possible differences in loading and related implications concerning failure rates for DMB and SMB configurations, there are other dimensions to bearing design and selection, such as cost and ease of servicing or replacement, which are factored in when design decisions are made. For example, a study relating drivetrain configuration to capital cost [20] found that a SMB configuration can result in a reduction in turbine capital cost of up to 3.5% compared to the DMB setup. Therefore, while hopefully illuminating in terms of understanding differing failure rates in the reported figures, the load analysis considered here should not be deemed conclusive in terms of overall optimum bearing selection.

4 | DRIVETRAIN MODELS

Finite element analysis (FEA) is often used to determine loading in drivetrain components. However, FEA techniques are computationally expensive and time consuming. The current work is looking to analyse loading across a large number of wind field conditions in order to try and determine global trends in main-bearing loads. Simpler models have therefore been developed which are suitable for analysing large numbers of loading time histories, while also having the added benefit of making the separation of cause and effect in results more straightforward. The parameters of these simple models were tuned using Romax FEA software in order to make them as realistic as possible. In the current paper both single main-bearing (SMB) and double main-bearing (DMB) configurations are considered, schematics of these two drivetrain types are shown in Figure 2 along with the reference frame used. In the SMB setup it is the single bearing present which reacts axial loads; in the DMB setup however, the axial loads can either be reacted by the forward or rear bearing. All of these configuration have been used for commercially available wind turbines and so all three setups are considered here. The damage modes discussed in Section 3 are all strongly dependent on out-of-plane and thrust reaction loads at the MB and so these forces will be focused on in the current work. Rotational frictional forces between bearing rolling elements and raceway (along with those stemming from gearbox interactions) are neglected in the current models, with shaft torques assumed to transfer through the bearing

without loss. Frictional forces and shaft torque (along with subsequent reactions at the gearbox) should certainly play a role in MB health, however, their influence should not significantly impact the out-of-plane bearing reaction forces and hence for the current work this simplification seems valid for the load types under investigation. As outlined below, the out-of-plane gearbox reactions are included in the current models as equivalent spring stiffness's.

Three dimensional hub loads (including both forces and moments) entering the drivetrain are decomposed into orthogonal components. In-plane pairs of forces and moments are then injected into drivetrain models of the form shown in Figure 3 and bearing reactions determined (equations for these reactions are derived in the following sections) for the vertical and horizontal planes separately, assuming independence of orthogonal force and moment directions. The shaft lengths L_1, L_3 and L_4 are those of a commercially available wind turbine of a similar power rating. The shaft lengths L_2 and L_5 are equivalent torque-arm lengths which, along with the spring stiffnesses, were tuned using Romax FEA such that, from the point of view of the main-bearing, they provide the same support reactions as would the remaining drivetrain components which lie beyond the main-bearing itself, including the gearbox trunnion supports. The force G is the gearbox weight in the vertical plane and zero in the horizontal plane. Forces along a given axis, i say, will be denoted by B_i for input forces and F_i for bearing reaction forces and, similarly, moments will be denoted by M_i. Therefore, the bearing reaction force F_z is determined from the in-plane pair $B = B_z$ and $M = -My$ with G equal to the gearbox weight. F_y is determined from $B = B_y$ and $M = M_z$ with G=0. Having determined reaction forces in the y and z axes the resultant radial main-bearing reaction force is then of magnitude,

$$F_R = \sqrt{(F_y)^2 + (F_z)^2}. \tag{1}$$

All axial loads are assumed to be reacted by the axially fixed bearing in each model and so $F_x = -B_x$ in each case (not shown in diagrams). Note that this study considers main bearing equilibrium loads in a quasi-static sense and for the DMB models a simplifying assumption of negligible deflections at the gearbox and bearings is applied, as such, the spring stiffness values are not specifically required for the current analysis. However, these same models will be used in future work where these values are required, and so full details are included here for the sake of completeness and continuity.

4.1 | Single Main-Bearing Model

For the case of a SMB the equation system is statically determinate for each in-plane force-moment pair and hence reaction forces can be solved for easily. This setup corresponds to the top model in Figure 3. Balancing moments about the gearbox gives,

$$M + (L_1 + L_2)B - L_2F = 0, \tag{2}$$

therefore, this can be rearranged in order to give the bearing reaction force, F, as,

$$F = \frac{M + (L_1 + L_2)B}{L_2}. \tag{3}$$

4.2 | Double Main-Bearing Models

The DMB models are both statically indeterminate and so a more sophisticated analysis becomes necessary. The DMB models are the bottom two in Figure 3. Forces and moments can be balanced in order to generate two equations, however for the DMB models there are three unknowns (e.g. F^a, F^b and the gearbox reaction force in DMB-1). In order to generate a third equation, thus making a solvable system, the method of double integration is used (see for example Chapters 7 and 8 in [21]). Since the two DMB models have identical solution methods, here only DMB-1 is considered for the sake of brevity. For DMB-1 we therefore arrive at the following system of three equations with three unknowns;

$$-F^a - F^b - F^g + G + B = 0 \tag{4}$$

$$-L_3F^b - (L_2 + L_3)F^g + (L_1 + L_2 + L_3)B + M = 0 \tag{5}$$

$$-\frac{F^a}{6}(L_2 + L_3)^3 + \frac{G}{6}(L_2 + L_3)^3 - \frac{F^b}{6}L_2^3 + \frac{F^a}{6}L_3^2(L_2 + L_3) - \frac{G}{6}L_3^2(L_2 + L_3) = 0 \tag{6}$$

Where Equations 4 and 5 result from force and moment balancing respectively, and Equation 6 results from double integration of the beam's deflection curve differential equation, under the assumption of zero deflection at the gearbox and each of the two main-bearings. F^g denotes the reaction

TABLE 1 Data for wind turbine model used for aero-elastic simulations.

Rated power	2 MW
Rotor diameter	80 m
Blade number	3
Hub height	61.5 m
Aerodynamic control	Pitch
Fixed/Variable speed	Variable
Controller	PI

PI, proportional integrator.

force at the gearbox, not shown in the diagram for the sake of simplicity. The system of equations generated can then be solved as follows: letting,

$$\theta_1 = -\frac{1}{6}(\mathsf{L}_2+\mathsf{L}_3)(\mathsf{L}_2^2+2\mathsf{L}_2\mathsf{L}_3) \tag{7}$$

$$\theta_2 = -\frac{\mathsf{L}_2^3}{6} \tag{8}$$

$$\theta_3 = \frac{\mathsf{G}}{6}(\mathsf{L}_2+\mathsf{L}_3)(\mathsf{L}_2^2+2\mathsf{L}_2\mathsf{L}_3), \tag{9}$$

and,

$$\psi_1 = -\mathsf{L}_3 \tag{10}$$

$$\psi_2 = -(\mathsf{L}_2+\mathsf{L}_3) \tag{11}$$

$$\psi_3 = (\mathsf{L}_1+\mathsf{L}_2+\mathsf{L}_3)\mathsf{B}+\mathsf{M}, \tag{12}$$

the following expressions solve the system of Equations 4-6 for the reaction forces;

$$F^b = -\frac{G+B+\frac{\theta_3}{\theta_1}+\frac{\psi_3}{\psi_2}}{\frac{\theta_2}{\theta_1}+\frac{\psi_1}{\psi_2}-1} \tag{13}$$

$$F^a = -\frac{\theta_2 F^b+\theta_3}{\theta_1} \tag{14}$$

$$F^g = -\frac{\psi_1 F^b+\psi_3}{\psi_2}. \tag{15}$$

5 | SIMULATION

Fully aero-elastic multi-body simulations of a 2MW wind turbine were performed in DNV-GL Bladed software. This modelling software combines Blade Element Momentum theory, aero-elastics and multibody dynamics and includes all inertial and gravitational loads. The 3D turbulent wind fields were generated in Bladed and in compliance with IEC standards [22] using a Kaimal spectrum. Relevant background and theory to generating these wind fields is discussed in [23]. Briefly: second order wind field statistics are captured in frequency space by a *spectral tensor* function, a function of wavenumber whose values characterise the energy and structure in the wind field. For a given spectral tensor model (the Kaimal spectrum being one) velocity components are determined by summing a set of coefficients, determined for that wind model, multiplied by randomising noise terms. Using different initial random number seeds it is possible to generate multiple (different) wind fields which share the same second order statistics both temporally and spatially.

In the current paper, wind fields are characterised by three parameters: hub-height mean wind speed, turbulence intensity and power law shear exponent. In order to give statistical significance to the results presented here, 6 (the minimum number required by IEC standards [22] for design certification) different 3D turbulent wind fields were generated for each possible combination of the following: mean wind speeds (10, 12, 16, 20 m/s), turbulence intensities (TI) (low, med and high as specified by the IEC [22]) and power law shear exponents (0.2, 0.6); a total of 144 wind fields.

The turbine was simulated in each of the generated wind fields and the hub loading, which includes gravitational and inertial forces, was extracted. Each of these simulations result in 10 minutes of hub loading time history. Note that for the sake of clarity, the sets of 6 loading time histories in wind fields with the same parameters will be referred to as Common Parameter Load Sets (CPLS).

6 | RESULTS

6.1 | Mean Loading

Mean loading was analysed across the various wind conditions and for each of the drivetrain models. For the 6 time histories in each CPLS, for a given reaction load, the mean load was determined for each of the six. These six mean loads were then averaged and these average values, along with standard deviations, are presented in Figures 4-7. This approach was taken in order to show consistency of the given mean loading in each type of wind field.

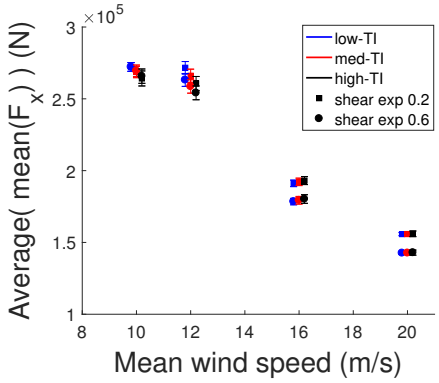

FIGURE 4 Mean axial loading and standard deviations across each CPLS for the axial-reacting bearing in each of the three models. Results are staggered about each wind-speed for clarity.

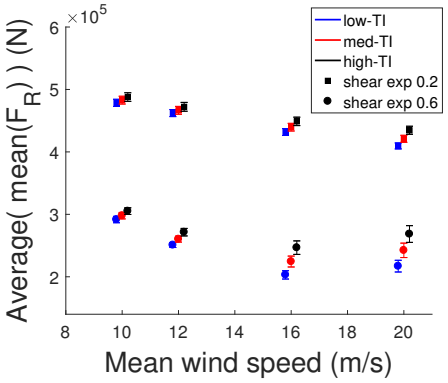

FIGURE 5 Mean radial loading and standard deviations across each CPLS in SMB model. Results are staggered about each wind-speed for clarity.

Figure 4 shows the mean loading result for axial loads F_x, which are the same for the axial loads on the axial reacting bearing in all three models. The axial loading can be seen to drop off rapidly at above rated wind-speeds. From Figure 1 it is clear that this is due to the turbine's operating strategy shedding both power and loads at higher wind speeds. In Figure 4 it is also clear that mean loading in given wind conditions is very consistent, as indicated by small standard deviations. Finally, it is of note that in above rated wind speeds the higher axial loads are seen for the lower shear exponent. This is due to the fact that for a power law shear profile, and for the current turbine size, an increase in shear exponent from 0.2 to 0.6, results in a decrease in the mean wind speed across the rotor. This has previously been shown to be the case in the context of tower loading [23].

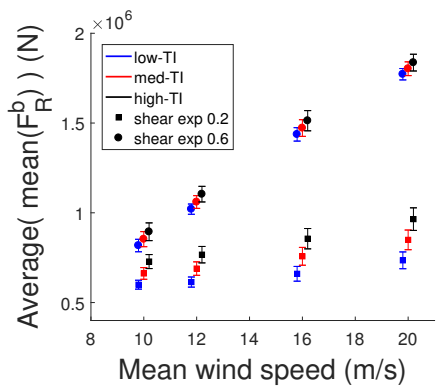

FIGURE 6 Mean radial loading and standard deviations across each CPLS in DMB-1 model. Results are staggered about each wind-speed for clarity.

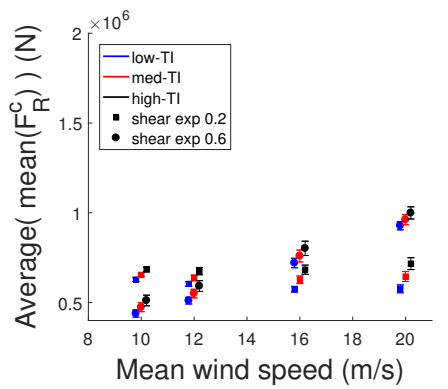

FIGURE 7 Mean radial loading and standard deviations across each CPLS in DMB-2 model. Results are staggered about each wind-speed for clarity.

Figure 5 shows the bearing mean radial loading results for the SMB model. As with the axial loads, the low shear exponent results in higher radial loading. This particular load has a high sensitivity to shear exponent, with TI also having an impact. For a given shear exponent and TI the mean radial main-bearing loading remains similar across the range of wind speeds. The mean loads within CPLS can also be seen to be fairly consistent, with small standard deviations in each.

Figures 6 and 7 then show mean radial loading across CPLS for bearings b and c respectively (equivalent to that of bearings d and a respectively). It is immediately clear that for the DMB case, the mean radial load behaviour is different. For bearing b (equivalently d) it is high shear which produces the largest mean radial loading, and the disparity between the loading for the two exponents increases with wind speed. A small sensitivity to TI is also present. These loads are also fairly consistent within each CPLS. For bearing c (equivalently a) the loading trends are more complicated again; as can be seen in Figure 7 the effect of wind shear is reversed in the higher two wind speeds as compare to the lower two. While shear exponent remains an important sensitivity factor, its effect here is less pronounced than was seen for bearing b (equivalently d) in Figure 6.

In terms of load magnitudes the results in Figures 5-7 show that mean radial loads are significantly larger for the DMB drivetrain models compared to SMB. Bearing b (equivalently d) sees the overall highest mean radial loads. These increased radial loads for DMBs make sense intuitively since when comparing the DMB and SMB models it is clear that, in either DMB setup, the bearings are reacting moments along shorter torque arms and hence the associated loads must be higher.

6.2 | Peak Loading

Peak loading was analysed across the various wind conditions and for each of the drivetrain models. For the 6 time histories in each CPLS, for a given reaction load, the peak load was determined for each of the six. These six peak loads were then averaged and these average values, along with standard deviations, are presented in Figures 8-11. As with mean loading, this approach was taken in order to show consistency of the given peak loads in each type of wind field.

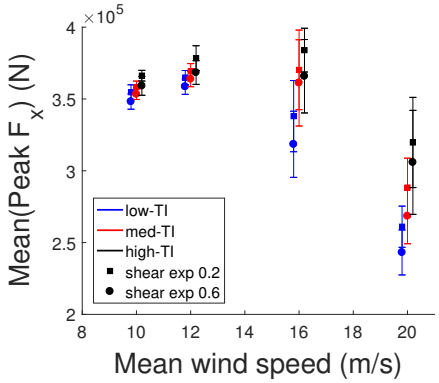

FIGURE 8 Mean-peak axial loading and standard deviations across each CPLS for all three models. Results are staggered about each mean wind-speed for clarity.

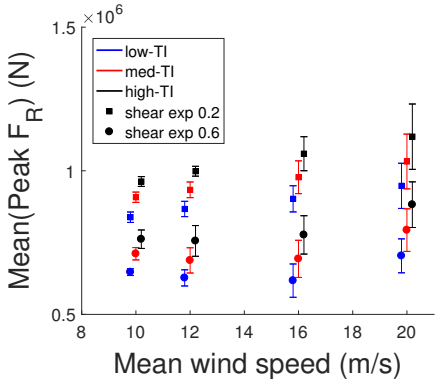

FIGURE 9 Mean-peak radial loading and standard deviations across each CPLS in SMB model. Results are staggered about each wind-speed for clarity.

Figure 8 shows the peak loading results for axial loads F_x, which are the same for the axial loads on the axial reacting bearing in all three models. As with mean axial loading, the peak loads can be seen to drop off at higher wind speeds. However, the other trends here are somewhat different; when considering peak axial loading Figure 8 shows TI to be the highest sensitivity factor, as opposed to SE (which was the more important factor when considering mean axial loads). Furthermore, the peak axial loads within each CPLS vary by a significant amount, as indicated by the large standard deviations in higher wind speeds.

Figure 9 shows the bearing peak radial loading for the SMB model. These peak loads generally increase in size and variability (standard deviations) as the wind speed increases. As with mean loading, the largest values seen here are from the low shear exponent. These peak load values are most sensitive to the SE, but there is also a significant effect coming from changes in TI.

Figures 10 and 11 then show peak radial loading across CPLS for bearings b and c respectively (equivalently d and a respectively). The results here qualitatively match those seen for mean loading on these bearings, with peak loads increasing with wind speed and shear exponent for bearing b (equivalently d) in Figure 10, and the change in loading behaviour with respect to shear exponent (mentioned previously) again apparent in the peak loads of bearing c (equivalently a).

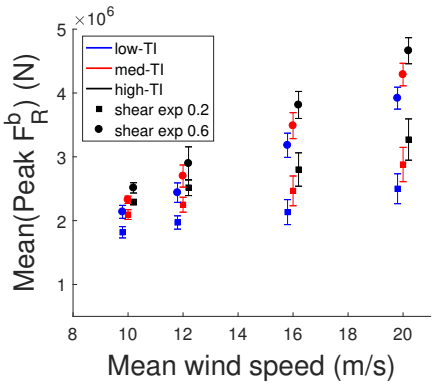

FIGURE 10 Mean-peak radial loading and standard deviations across each CPLS in DMB-1 model. Results are staggered about each wind-speed for clarity.

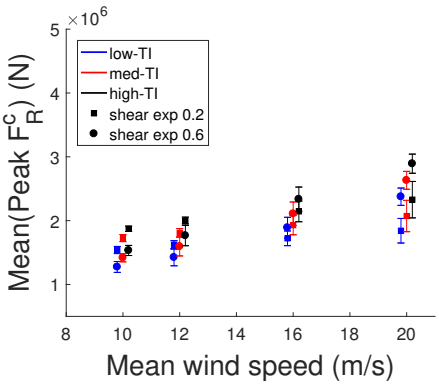

FIGURE 11 Mean-peak radial loading and standard deviations across each CPLS in DMB-2 model. Results are staggered about each wind-speed for clarity.

Unsurprisingly, based on mean loading results, the peak radial loads for the DMB models are significantly higher than those seen for the SMB model.

6.3 | Load Ratios

Apart from the loads themselves, certain combinations of loads have been found to have implications for bearing health. The most important of these, and the one considered in the current paper, is the axial-to-radial load ratio F_x/F_R.

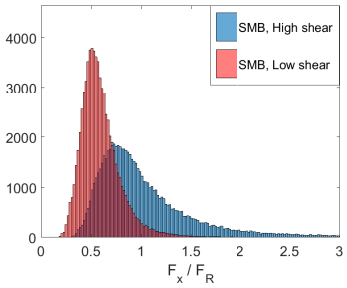

FIGURE 12 Histograms of load ratios for SMB model in 10 m/s mean wind speed and medium TI.

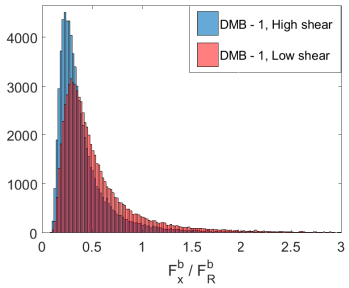

FIGURE 13 Histograms of load ratios for DMB-1 model in 10 m/s mean wind speed and medium TI.

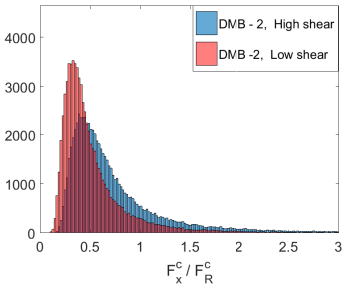

FIGURE 14 Histograms of load ratios for DMB-2 model in 10 m/s mean wind speed and medium TI.

An analysis of this load ratio is meaningful for the axial load reacting bearings (b and c in DMB-1 and DMB-2 respectively), the non-axial reacting bearings have a theoretically constant axial to radial load ratio of zero. Figures 12-14 shows histograms of the load ratios across all CPLS with mean wind speeds of 10m/s and medium TI for the three main-bearing models. The load distributions can be seen to appear Weibull in nature. The distributions of load ratios have the same Weibull type shape across all wind speeds and TIs and so in order to make comparisons we will present the mean load ratios from simulation in each set of wind field parameters.

Figure 15 shows the mean load ratios for the SMB model. Two features stand out in this figure. First, it is clear that the SE is the single most important factor in determining the mean load ratio for the SMB reaction forces. Second is that there is noticeably different load ratio behaviour between regions where pitch control is active and regions where it is not, with the transition between these two regimes captured by the high shear and high turbulence intensity point with 12 m/s mean wind speed. Generally, the mean load ratios experienced by the main-bearing are not sensitive to TI, except in the pitch active regions (16 and 20 m/s) and with a high SE. Finally, for high wind speeds the highest (and potentially most damaging) load ratios occur in high shear and low turbulence intensity conditions.

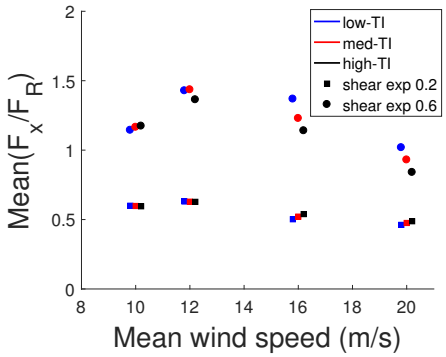

FIGURE 15 Mean load ratios across the spectrum of wind conditions for SMB model. Results are staggered about each wind-speed for clarity.

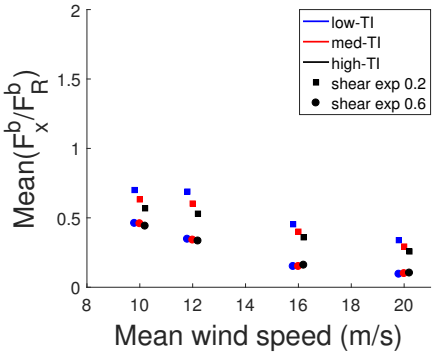

FIGURE 16 Mean load ratios across the spectrum of wind conditions for DMB-1 model. Results are staggered about each wind-speed for clarity.

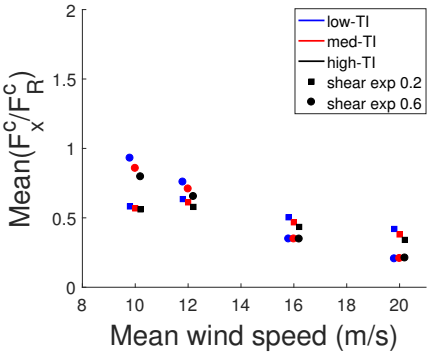

FIGURE 17 Mean load ratios across the spectrum of wind conditions for DMB-2 model. Results are staggered about each wind-speed for clarity.

Figures 16 and 17 then show the mean load ratios for the DMB models. It is clear that the load-ratio behaviours for both DMB-1 and DMB-2 have changed significantly as compared to the SMB setup. In DMB-1, the maximum mean load-ratios seen by bearing b are much lower than those seen by the SMB bearing, however, there are wind conditions in which the load-ratios for bearing b are larger than those seen by its SMB counterpart. The trend seen by the SMB when moving from low to high shear is reversed in DMB-1 case, with low shear producing the largest load ratios. It is in the low shear case also in which the mean load-ratios on bearing b are most sensitive to turbulence intensity at each simulated wind speed. This sensitivity disappears in high shear where mean load-ratios are more tightly clustered. Across all wind speeds, the most damaging conditions, in terms of load ratios for DMB-1, is the combination on low SE and low TI.

In DMB-2 (Figure 17), the load ratios are again generally lower than in the SMB case. The DMB-2 load ratios on bearing c are generally higher than those seen by bearing b in DMB-1. Here there is also present the switching in terms of SE which was seen previously in the mean and peak radial loads for the current model. Note that in the current results the load ratios which are most sensitive to TI are whichever are highest with respect to SE. This is high SE conditions at lower wind speeds and low SE at higher wind speeds.

The generally lower load-ratios seen in the case of DMB configurations can be explained in terms of the generally higher radial loads seen by these drive-train configurations, as shown in the mean and peak loading results. Since the axial loading remains unchanged, increased radial loads will decrease the load-ratios.

7 | DISCUSSION

The results presented here demonstrate the enormously variable nature of main-bearing loads for each of the three drivetrain models. The considered loads were all shown to be highly sensitive to wind field parameters and this challenges the assumption (e.g. made in some works [8]) that

main-bearing loads can be linked to power, and hence wind-speed, alone. Generally the SMB was shown to be the most sensitive to changes in wind-field parameters, however the radial loads on both of the DMB models were found to be significantly larger than for the SMB in terms of both mean and peak loading. Assuming load ratios to be an important factor in main-bearing damage and health, from the results here there is no clear optimal configuration across all three models and wind conditions. While the SMB model definitely see the highest load ratios overall, there are specific wind conditions where the DMB load ratios are higher, for example in low shear and at mean wind speeds of 10 and 12 m/s the DMB-1 axial reacting bearing can be seen to exhibit higher mean load ratios than its SMB counterpart. This suggests that choosing an optimal drivetrain configuration to minimise axial-to-radial load ratios may depend on the site specific conditions of a proposed wind farm.

In terms of the question posed at the beginning of this paper, the results presented in the previous section clearly demonstrate that a large range of different load conditions are experienced by main-bearings across the turbine's operational envelope; furthermore, there were shown to be strong links between main-bearing loads and the characteristics of the incident wind-field. Importantly, these results highlight the need for further research into wind turbine main-bearing operational loading in order to allow for better design decisions. A more thorough understanding of loading might also inform new O&M techniques for main-bearings.

8 | CONCLUSIONS

In this paper the lack of research, performed to-date, focusing on wind turbine main-bearings was highlighted and compared to the large literature which considers gearbox bearings in wind turbines. Inroads to filling this knowledge gap were made by studying three simplified drivetrain models and the resultant main-bearing loads when realistic hub loads were injected; these bearing loads were then related to incident wind field characteristics, with a goal of understanding the range of load conditions experienced by wind turbine main-bearings and links to wind field characteristics. The input hub loads were generated using Bladed software which performs fully aero-elastic simulations in 3D turbulent wind fields. Mean and peak loads in the axial and radial planes were analysed along with the axial to radial load-ratios. Loading results demonstrate that a wide range of load conditions are present across different operating points and that main-bearing loading is strongly linked to the characteristics of the incident wind field. In more detail, the following results were obtained which address the question posed at the beginning of this paper, both in general and with respect to the investigated main-bearing types:

Axial loads for the fixed bearing in each model were found to be most sensitive to mean wind speed. This is due to the wind speed dictating how much thrust is present on the rotor and when pitching is activated in order to shed loads. Peak axial load results showed increasing variance and sensitivity to shear and turbulence as mean wind speed increases. Mean radial loads for the SMB model were found to be most sensitive to changes in the shear exponent values used here, with changes in wind speed and turbulence resulting in comparable changes to mean radial loads. In the SMB case the higher value of shear resulted in lower mean (and peak) radial loads, indicating that shear effects can 'lift' the rotor from the main-bearing's points of view, acting contrary to gravitational forces. As with axial loads the SMB peak radial loads were found to have variances and sensitivities to shear and turbulence which increase with mean wind speed. For the DMB cases the radial load behaviours are very different. Both DMB bearings see significantly higher radial loads compared to the SMB model. For the front DMB bearing, high shear produces the highest radial loads in terms of both mean and peak values and the disparity between loads as a results of an increase in shear exponent becomes larger as mean wind speeds increase. The rear DMB bearing on the other hand has a 'switching point' present whereby the value of shear which results in higher mean and peak radial loads changes at an intermediate wind speed value. This case also displays a much reduced sensitivity to values of shear exponent when compared to the front DMB bearing. For both front and rear DMB bearings, increases in turbulence levels can be seen to result in higher mean and peak radial loads.

Load ratio results were also investigated. It was found that the SMB drivetrain load-ratios were the most sensitive to wind field characteristics, while also seeing the highest (and potentially most damaging) values. The DMB configurations on the other hand had lower sensitivities and values in terms of load-ratios, likely due to their considerably increased radial loads. For the SMB case the highest load ratios were found to occur for the larger value of shear exponent. For DMB-1 this situation was found to be reversed, and for DMB-2 there is again a 'switching point' where the value of shear exponent resulting in the highest load ratios changes at an intermediate wind speed value. Generally, but not universally, increases in turbulence intensity can be seen to decrease load ratios for each of the three models.

20 year failure rates determined from operational data were also presented which showed roughly double the frequency of failures for a SMB design as compared to a DMB design. With respect to the load modelling results, a driver for these figures could be the higher load-ratios seen by the SMB model. However, it is important to note that while the SMB model saw higher load ratios, this was driven by higher radial loads experienced by the DMB models. Hence, for this conclusion to hold it would be necessary for load ratios, as opposed to individual load magnitudes, to be the main driver of main-bearing damage. The relative importance of these two factors to main-bearing health should therefore be considered as part of future work in this area.

Overall, this work has demonstrated a high variability in main-bearing loads across a wind turbine's operational envelope, and a strong link to incident wind field characteristics. Load characteristics were also found to differ significantly for different main-bearing types. These results indicate further work is necessary in order to better understand these relationships, while also suggesting that optimal drivetrain main-bearing design may require information about wind field conditions at a proposed wind farm site.

ACKNOWLEDGEMENTS

The authors would like to thank the anonymous reviewers for their helpful insight and comments.

References

1. Sethuraman L, Guo Y, Sheng S. *Main bearing dynamics in three-point suspension drivetrains for wind turbines*. NREL, AWEA WINDPOWER, Orlando, 2015.

2. Hart E, Turnbull A, McMillan D, Feuchtwang J, Golysheva E, Elliott R. Investigation of the relationship between main-bearing loads and wind field characteristics. *J. Phys.: Conf. Ser.* **926** 012010.

3. Hart E, Turnbull A, McMillan D, Feuchtwang J, Golysheva E, Elliott R. *Futher investigation of the relationship between main-bearing loads and wind field characteristics*. EERA DeepWind, Trondheim, Norway 2018.

4. Qu Y, Chen C, Zhou B. Study on fault diagnosis on wind turbine main bearing based on finite element analysis and wavelet analysis. *Advanced Materials Research* 2011; DOI: 10.4028/www.scientific.net/AMR.308-310.1264.

5. Wang Y F, Kootsookos P J. Modelling of low shaft speed bearing faults for condition monitoring. *Mech. Sys. and Sig. Proc.* 1998; 12(3),415-426.

6. Ghane M, Nejad A. R, Blanke M, Gao Z, Moan T. Statistical fault diagnosis of wind turbine drivetrain applied to a 5MW floating wind turbine. *Journal of Physics: Conference Series (Online)*, 753, [052017]. DOI: 10.1088/1742-6596/753/5/052017

7. Zhang Z. Automatic fault prediction of wind turbine main bearing based on SCADA data and artificial neural network. *Open Journal of Applied Sciences*, 2018, 8, 211-225. DOI: 10.4236/ojapps.2018.86018

8. Xiaopin Y, Haitao W, Yang Z, Zhiying Z. *The research on the dynamic lubricating control system of wind turbine's main bearings*. IEEE International Conference on Power and Renewable Energy, 2016.

9. Meadows B, Shapiro J. *Data-driven main bearing maintenance strategies to reduce unplanned maintenance costs*. Wind Systems, inFOCUS: WINDPOWER, 2016.

10. Zheng J, Ji J, Yin S, Tong V. C. *The load distribution of the main shaft bearing considering combined load and misalignment in a floating direct-drive wind turbine*. E3S Web of Conferences 64, 07009 (2018). DOI: 10.1051/e3sconf/20186407009.

11. Baldwin B. *Increasing bearing reliability in a main shaft support system*, White Paper, Timken.

12. Dabrowski D, Natarajan A. Identification of loading conditions resulting in roller slippage in gearbox bearings of large wind turbines. *Wind Energ.* 2017; 20:1365-1387. DOI: 10.1002/we.2098.

13. Guo Y, Keller J. Investigation of high-speed shaft bearing loads in wind turbine gearboxes through dynamometer testing. *Wind Energ.* 2018;21:139-150. DOI: 10.1002/we.2150.

14. Gould B J, Burris D L. Effects of wind shear on wind turbine rotor loads and planetary bearing reliability. *Wind Energ.* 2016; 19:1011-1021. DOI: 10.1002/we.1879.

15. Jiang Z, Xing Y, Guo Y, Moan T, Gao Z. Long-term contact fatigue analysis of a planetary bearing in a land-based wind turbine drivetrain. *Wind Energ.* 2015; 18:591-611. DOI: 10.1002/we.1713.

16. Y. Liang, Z. An, B. Liu. *Fatigue life prediction for wind turbine main shaft bearings*. International Conference on Quality, Reliability, Risk, Maintenance, and Safety Engineering (QR2MSE), July 2013.

17. Gurumoorthy K, Ghosh A. Failure investigation of a taper roller bearing: A case study. *Case Studies in Engineering Failure Analysis* 1 (2013) 110-114.

18. Harris T A, Kotzalas M N, Yu K W On the Causes and Effects of Roller Skewing in Cylindrical Roller Bearings. *Tribology Transactions*, 41:4,572-578, 1998.

19. Kotzalas M N, DOLL G L. Tribological advancements for reliable wind turbine performance *Phil. Trans. R. Soc. A* (2010) 368, 4829-4850.

20. Guo Y, Parsons T, Dykes K, King R. N. A systems engineering analysis of three-point and four-point wind turbine drivetrain configurations. *Wind Energ.* 2017;20:537-550. DOI: 10.1002/we.2022

21. Benham P P, Crawford R J, Armstrong C G. *Mechanics of Engineering Materials.* 2nd ed. Essex: Pearson Prentice-Hall; 1996.

22. IEC. *Wind turbine design requirements*. IEC 61400-1:2005(E), 2005.

23. Hart E, Keegan M, McMillan D. *A lookup table approach to determining wind turbine operational fatigue loading from wind field measurements*. ASRANet, International Conference on Offshore Renewable Energy, Glasgow, UK, 2016.

How to cite this article: Edward Hart, Alan Turnbull, Julian Feuchtwang, David McMillan, Evgenia Golysheva, and Robin Elliott (<year>), <journal title>, <*journal name*> <year> <vol> Page <xxx>-<xxx>